Contents

Chapter 1

Plasma source description and electric characterization

Plasma Coagulation Controller (PCC) developed at RFX is a DBD cold plasma source that produces plasma at atmospheric pressure. The entire design is developed to garantee the flexibility necessary to easy application on target. In this chapter we describe the source functioning scheme and characterize it.

1.1 General source description

PCC functions applying a fast high voltage pulse (from 2 to 10 kV) to a cyilindrical electrode covered by pyrex glass that works as the dielectric used to produce plasma in DBD conditions ([1]). The electrode is positioned along the axis of a nozzle where we insert neutral gas, a pure noble gas sometimes mixed with other gasses, that allows to start the discharge. It is possible to put a second electrode formed by a conducting ring around the nozzle, that we can set to ground voltage or other voltage values, to modify the electric field if necessary.

When we start the voltage pulse, the electrode generates an electric field that ionizes the gas producing plasma with low free charge density thanks to the glass dielectric. Plasma forms a column of glowing gas, the plasma plume, that goes out from the nozzle exit and travels in the air outside, until it reaches a certain lenght or a target, as in figure 1.1. The plume is formed by cold plasma, it can be touched whitout a relevant increase of temperature on the skin or any other danger.

PCC development goes through different designs (an example of the first one in [2]), for this study we use two different prototypes for the head, **A** and **B**, with same concepts and little differences.

In both models we have the high voltage controller separated from the head where plasma is produced, the first one controls the trigger for the voltage pulse, the second one is where we produce plasma. The controller contains power cables and circuits and an Arduino Leonardo that controls pulse repetition rate and amplitude, as explained later. The head is a cylinder 30 cm long with diameter of 8 cm, where are mounted three

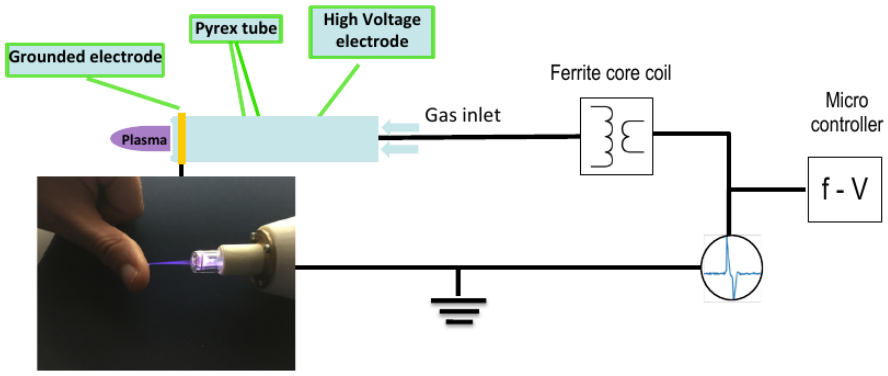

Figure 1.1: Scheme of the source. The micro-controller on the right sends a trigger signal to produce variable voltage on the coil mounted in the head, that produces an high voltage pulse on the electrode. The electric field ionizes the neutral gas and produces the plasma plume in the picture. The grounded ring around the nozzle is removable.

coils with three *N87* ferrite cores of dimensions $32 \times 16 \times 9\,\text{mm}$ and induttance $2.3\,\mu\text{H}$ ([3]). The spire ratio between primary and secondary circuit on the resulting coil is of 1/30. On one end of the head there is the driver circuit that receives an optical signal from the controller, that is the trigger signal for voltage pulse; on the other end there is the electrode. The driver circuit is connected with the primary circuit of the coil, the electrode to the secondary circuit. When the controller sends the trigger, there is a voltage variation on primary circuit that produces the voltage pulse on the electrode. Controller and head are connected only with power cables for driver circuit and an optical fiber that sends the trigger for the voltage pulse.

Gas is inserted trough a separated channel that goes from one end of the source to the other end near the electrode. The nozzle at the end of the head can be selected between different materials and shapes. For this study we utilize a plastic nozzle that expels plasma through a cylinder with diameter of 1 mm and a cylindrical glass nozzle that shrinks at the end, until a diameter of 5 mm.

Prototype **A** is the first version used during this work, prototype **B** is the latest one. Generally the second one is developed with higher ionization efficiency, principal differences are:

- they have different geometries for the coils inside the head, so prototype **B** can produce higher voltage peak values;
- prototype **A** has positive voltage pulse polarity while prototype **B** has negative voltage pulse polarity;
- prototype **A** presents a problem of neutral gas diffusion in the area where there are the coils, in prototype **B** the two areas are not in communication (except for the electric connection of the electrode).

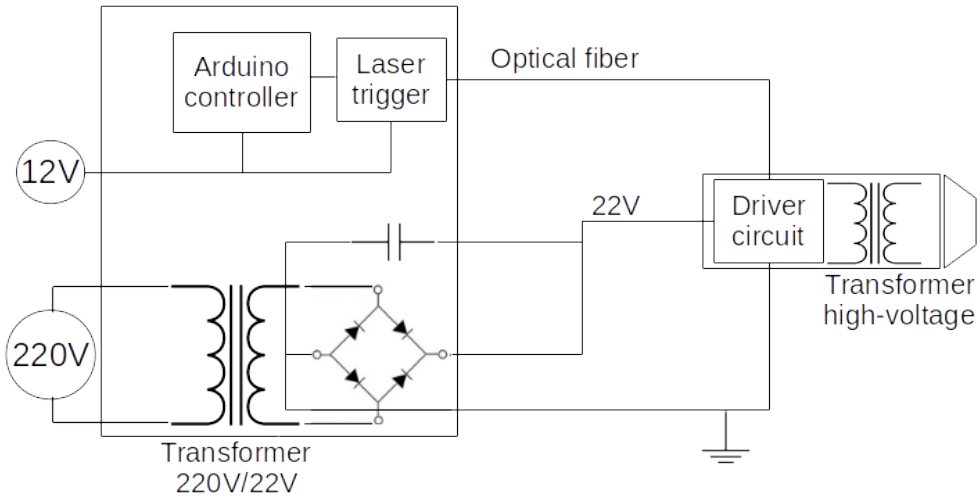

Figure 1.2: Electric scheme of the source. On the left there is the controller, on the right there is the head.

1.2 Electric scheme

In this chapter we discuss development of PCC eletcric scheme and its characterization. To produce plasma as DBD, in air, with helium or argon as ignition gasses, it is necessary to apply high voltage differance in short distances, resulting in high electric field. It is common to produce electric fields with fast voltage pulses for various uses, including jet or DBD plasma production ([4], [5], [6])), the scheme that we use outputs a voltage pulse with an amplitude from 1 kV to 10 kV and pulses frequencies from 5 kHz to 60 kHz.

One representation of the electric scheme is in figure 1.2. As we explained before, the circuit divides in two parts: the controller, with power task and voltage pulse settings, and the head, where we ionize the gas and create plasma.

Line divides in:

- **Power line** : the controller is connected to a 220 V AC (50 Hz) power line. This signal goes in a transformer that reduces voltage value and to a diode bridge that rectifies the signal, resulting in an output of 22 V DC. This voltage powers the Driver Circuit on the head.

- **Arduino and trigger** : Arduino and a laser are connected to a power line at 12 V. One of the Arduino analogical outputs sends a PWM wave to the laser trigger, that transmits an optical signal with the same duration and pulse repetition rate of the PWM through an optical fiber. The fiber ends on a photodiode installed on the driver circuit that works as a switch to trigger the voltage pulse. With this setup pulse repetition rate and pulse amplitude are set by Arduino and the high voltage signal that circulate on the head is entirely decoupled from the controller, avoiding problems of signal reflection on the power line or the Arduino.

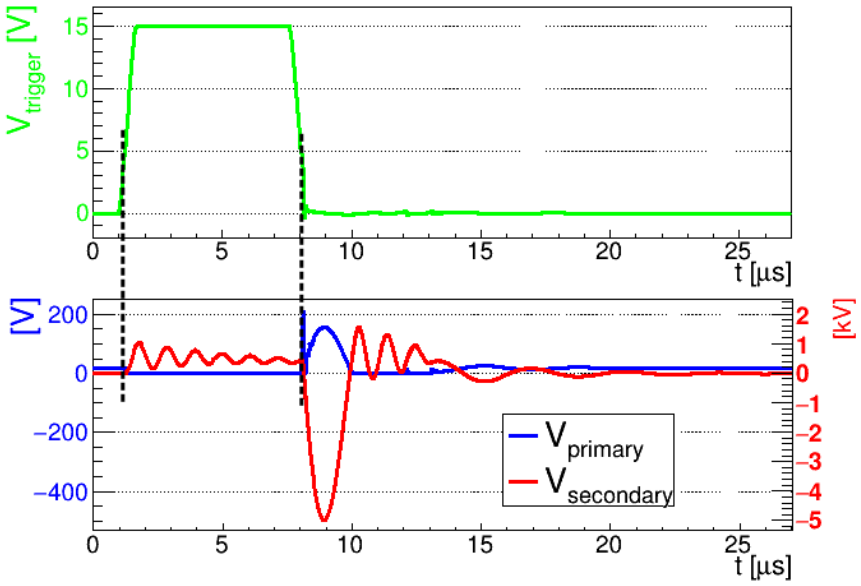

Figure 1.3: Scheme of signal propagation. Top in green there is the PWM trigger signal; bottom in blue there is the voltage of primary circuit with values in volts, in red the voltage of secondary circuit with values in kilovolts.

- **Head** : on the driver circuit there are the photodiode, a capacitor and a MOSFET that works as a switch for conductive and charging phases of the circuit. When the photodiode measure the laser signal voltage goes from power value to 0 and the capacitor starts charging. When the trigger signal ends, the voltage goes back to power value and the variation leads to a peak of thousends V on the output of the secondary circuit, connected to the electrode. Pulse repetition rate, f, is set precisely by the Arduino, PWM duration is set giving the opening time of the MOSFET, i.e. the duration of the charging time of the capacitor.

We present an example of voltage values on relevant components in figure 1.3, obtained with a simplified scheme with Spice. Once the PWM trigger starts, voltage on the primary goes from power value to 0, after 6 µs the PWM signal ends, and the output of the secondary circuit shows a peak of -5000 V and width of 1.2 µs. A longer PWM implies a longer charging time and an higher voltage. Ultimately, amplitude of the pulse is proportional to the width of the PWM signal and we can calibrate source peak output V_p in function of it Δt for every pulse repetition rate f. It is necessary to note that when we end the charging phase, at the end of the PWM signal, we have a voltage peak also on primary circuit with amplitude of 150 V and several oscillations of the same amplitude on the secondary. Those could influence the output behavior if we set pulse repetition rates too high, i.e. for values that would result in signal periods comparable to Δt.

We will study and compare output parameters for the two prototypes.

1.3 Output characterization

The electric field generated by the electrode define plasma creation and discharge features. We want to study the dependency of plasma behavior from voltage peak value and from pulse repetition rate, f. In addition, medical application of plasma requires low current intensity on target, in this study it's measured current intensity flowing on a copper sheet targeted by the plasma plume at a certain distance. Ultimately the different parameters for the measures are: Δt, opening time of the MOSFET in the circuit that is proportional to voltage peak value, and f, pulse repetition rate.

We measure voltage signals with a voltage probe (*hv probe*) built for high voltage measurements *Tektronix P6015A*, with an attenuation factor $\times 1000$. The voltage output from secondary circuit is taken right before the connection between secondary circuit and electrode. Current signal are measured with *Tektronix CT2* current probe for current measurements. This probe have an output of 1 mV for a current of 1 mA. We observe both signals with a *Yokogawa DL9040* oscilloscope, that is capable to store the total waveform that we measure.

We first take measurements without gas flow to characterize output voltage of the circuit, after we set an helium flow of 2 L/min, to measure the output in presence of plasma. For both conditions we measure outputs changing Δt for different repetition rate f. We measure also the mean current intensity over a time period, i.e. an effective current intensity I_{eff}, to evaluate plasma application's effects over a longer time period.

Every lenght measure is done with a decimal caliper, that gives a measurement uncertainity of 0.1 mm.

1.3.1 Measurements without gas

We set a repetition rate f and measure voltage signal for different values of the opening time Δt in the operational range. To assure that a voltage pulse ends before another starts, this range is different for different f: if we have more pulses in a given time and take into consideration pulse oscillations, the range of possible Δt is smaller for higher rates. A typical voltage waveform is in figure 1.4 (a). We want to verify proportionality between amplitude of the peak, V_p, and Δt, for different f. The signals are analyzed with a low-pass filter where we evaluate their Fourier Power Spectrum (using ROOT C++ libraries [7]) and reconstruct the signal without higher frequencies, to exclude noise fluctuations. The reconstructed peak is an asymmetric function in time as in figure 1.4 (b) that we fit with a Landau function [8] and obtain peak value and position. The error on the measure is evaluated adding contributes from the low-pass filter.

Results are shown in figure 1.5 for prototype **A** and **B**. For **A** we can see a linear behavior for $4 \leq \Delta t \leq 16\,\mu$s, with peak values from 2.02 ± 0.01 to 9.25 ± 0.05 kV; for larger Δt the relation is not linear. The upper limit on Δt is given by the need of a minimum time interval between two pulses. Also for **B** we can see a linear behavior, but with higher values: for $1 \leq \Delta t \leq 8\,\mu$s voltage peak goes from 3.66 ± 0.06 to 11.76 ± 0.22 kV. With this source the upper limit for Δt is chosen considering the maximum voltage value sustainable by the dielectric. To avoid the risk of dielectric breakdown we set the maximum

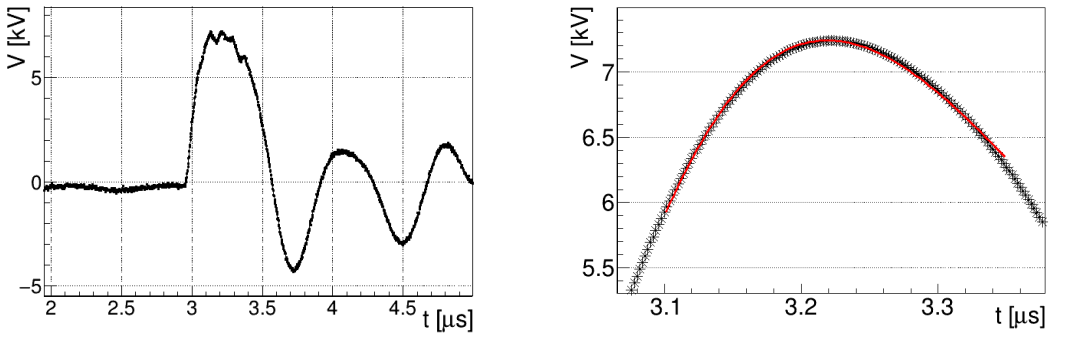

(a) Voltage peak example.

(b) Zoom on peak fit.

Figure 1.4: Example of voltage measurements with prototype **B** for $f = 5\,\text{kHz}$ and $\Delta t = 4\,\mu\text{s}$ (a) and its fit to estimate peak value and time (b).

opening time for prototype **B** at $\Delta t = 8\,\mu\text{s}$.

Voltage output doesn't show significative differances changing repetition rate. To confirm this observation we fit data with a linear function in the range $0 - 16\,\mu\text{s}$ for **A** and range $0 - 8\,\mu\text{s}$ for **B**. Parameters resulting from the fit are compared as in figure 1.6. Values are displaced with random distances from the mean value, so it can be concluded that the behavior is not defined by the repetition rate.

1.3.2 Measurements with gas

We introduce helium, with a flow of $2\,\text{L/min}$, at the end of the head near the electrode, producing plasma in DBD conditions. We want to study how voltage value changes with plasma introduction and the intensity of current carried by plasma on a conductive target. To assure safety of plasma application we want to avoid large current intensities with possibility of arc formation. Studies of conditions for DBD discharges and arc transitions ([9], [10], [11]) suggests that for fast pulses it's safe to have current intensity $< 10\,\text{mA}$.

Current intensity is measured with a copper sheet of dimensions $10\,\text{mm} \times 10\,\text{mm} \times 1\,\text{mm}$. The plasma plume impacts on the sheet that is connected to the current robe that converts the signal in a voltage measurements that we can read on the oscilloscope. We are measuring low current intensities so we have to pay attantion to cables shielding, decreasing noise. THe relation between current intensity and target distance is studied in [2]. In this work we choose a distance between target and electrode around typical values for treatments: $10\,\text{mm}$ for prototype **A** and $15\,\text{mm}$ for prototype **B**.

In figure 1.7 we present a measure for $\Delta t = 8\,\mu\text{s}$ and $f = 5\,\text{kHz}$ with prototype **B**. For both sources there is a current peak in correspondence of voltage pulse, that increases with voltage. However for prototype **B** there are measurements where the peak is so low that it is covered by noise.

Data analysis is the same described before, for both voltage and current values. Results are shown in figures 1.8 and 1.9, measurements where the current peak is not

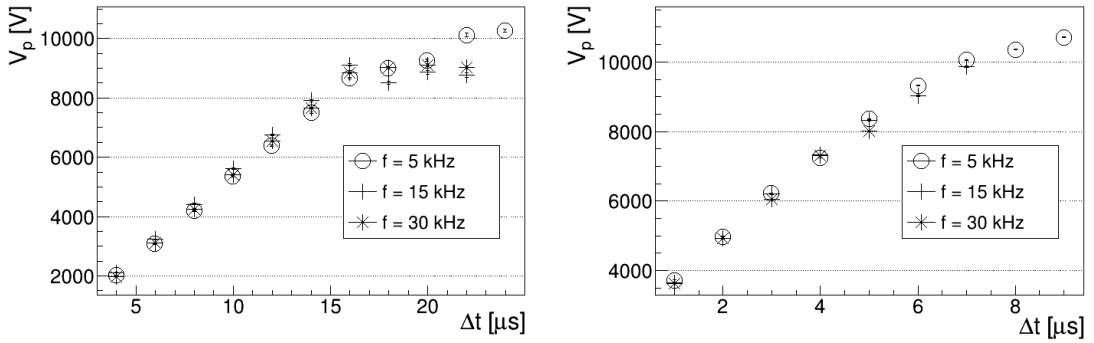

(a) Source A **(b)** Source B

Figure 1.5: Absolute voltage peak values of secondary circuit output in function of Δt at different f, for both prototypes. As we can see voltage peaks show linear behavior for $\Delta t \leq 15\,\mu s$.

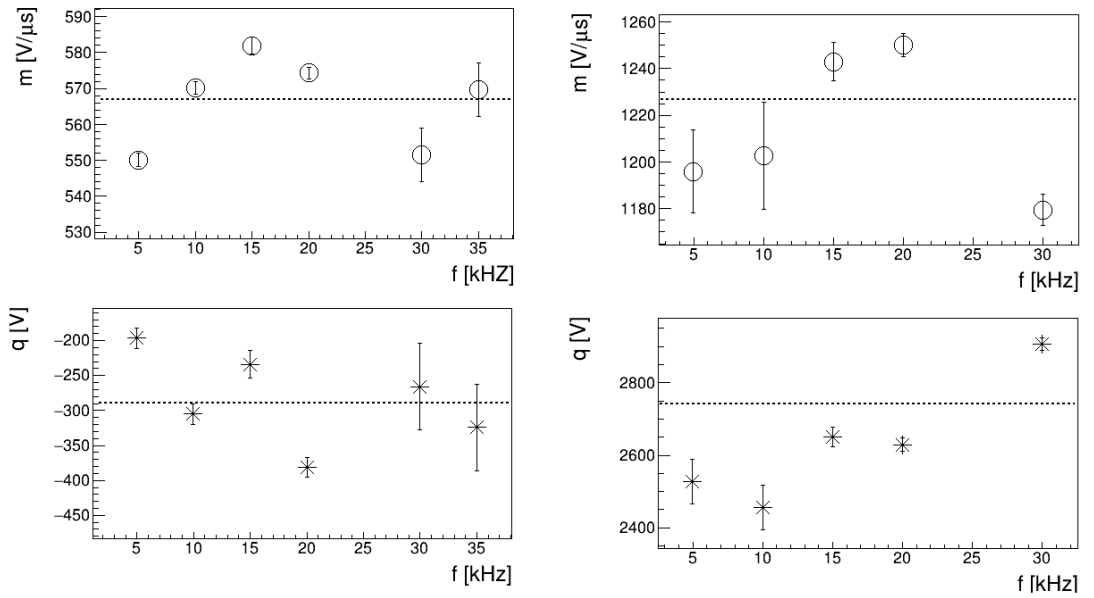

(a) Source A **(b)** Source B

Figure 1.6: We fit voltage peak in function of Δt with a linear function $V_{peak} = m\Delta t + q$, in figure we present fit parameters at different repetition rates for both sources. Dashed line is the average value of the parameter. There isn't a specific behavior in parameters, so we conclude that output voltage doesn't depend on pulse repetition rate.

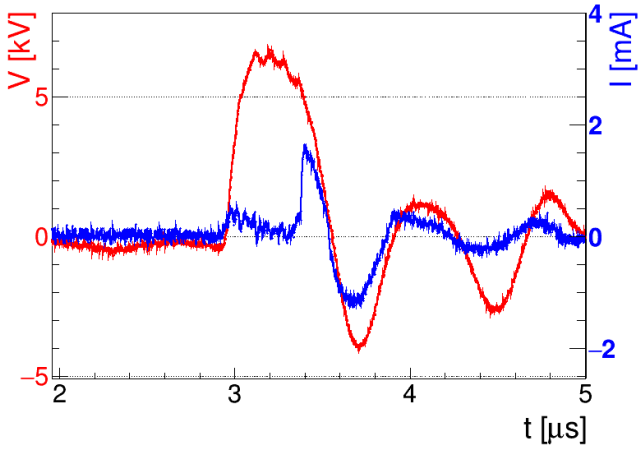

Figure 1.7: Example measurements with prototype **B** for $f = 5\,\text{kHz}$ and $\Delta t = 3\,\mu\text{s}$

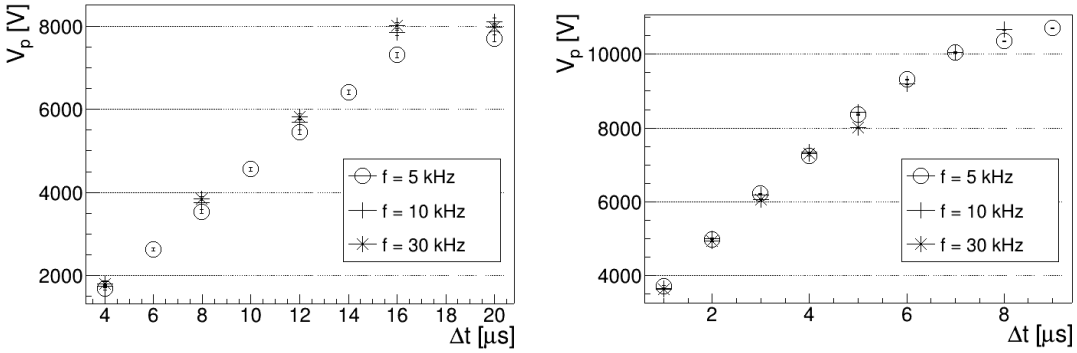

(a) Source A **(b)** Source B

Figure 1.8: Absolute voltage peak values of secondary circuit in function of Δt at different f, with an helium flux of 2 L/min, for both sources.

distinguishable from noise are excluded from plots.

Voltage peaks are lower then values without gas. It is an expected behavior if we consider the plume as an additional resistive load at the end of the circuit ([12]). Also for this measures we observe a linear dependency between voltage and Δt for $V_p \leq 10\,\text{kV}$, we can again compare linearity for different f. Current intensities increase as voltage and are higher for prototype **A**, as expected given different distances electrode-target. Analysis of linearity also for those measures can show if there is a different behavior changing pulse repetition rate. Figures 1.10 and 1.11 shows results of the linearity study for different pulse rates.

For voltage fit we find parameters scattered around their average value for both sources, confirming the hypotesis that voltage growth is independent from pulse repetition rates. For prototype **A** we find the voltage average increase $m_V = 0.366 \pm 0.001\,\text{kV}/\mu\text{s}$,

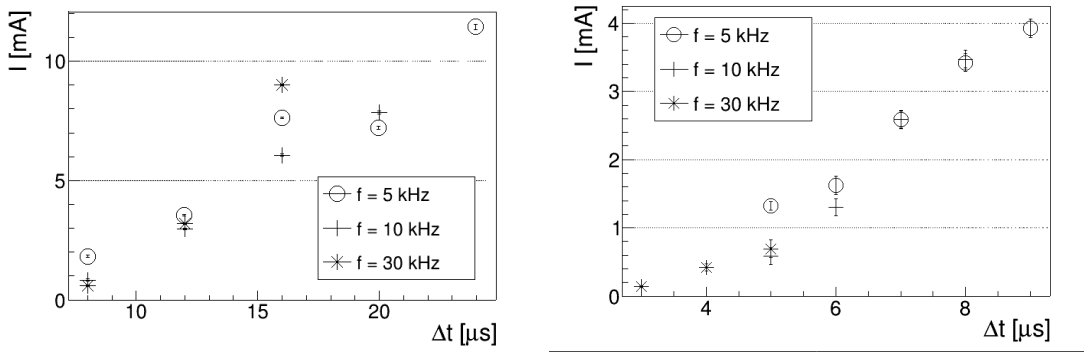

(a) Source A **(b)** Source B

Figure 1.9: Absolute current peak values measured with helium flux of 2 L/min, on a copper target, in function of Δt at different f, for both sources.

for prototype **B** $m_V = 1.145 \pm 0.008\,\mathrm{kV/\mu s}$, higher, as explained before.

Current values shows a different behavior: in prototype **A** we find a increasing parameters with increasing frequencies, in prototype **B** data are more scattered and we couldn't extrapolate a behavior. Despite this behavior the slope is in the same range of values for both prototypes, with a maximum for **A** of $m_I = 1.10 \pm 0.01\,\mathrm{mA/\mu s}$ and for **B** of $m_I = 1.04 \pm 0.17\,\mathrm{mA/\mu s}$.

The parameter trend in prototype **A** could suggest a variation of reaction parameters happening inside the plasma. If we have more ionization reactions with higher repetition rate, we would have higher charge densities and measure more current intensity. Due to low signal to noise ratio in measures for prototype **B**, it is not possible to esclude a relation between current slope and repetition rate for this source, however it is established a maximum limit value to take into consideration when using the device.

Time intervals From voltage and current waveforms we can also extrapolate informations on time width of those signals. They can be defined as the FWHM of measured peaks, evaluated as the time when we measure half of tension or current maximum value. As the characterization of the sources shows an almost equal behavior, this study is made only for the latest version of it prototype **B**, that's the only one used in the following chapters. Results are shown in figure 1.12. For every repetition rate there is a quadratic behavior of voltage widths with a minimum for a $\Delta t = 5\,\mu\mathrm{s}$. It is possible to give an estimation of pulse width with a mean value between this minimum and maximum values obtained for $\Delta t = 1\,\mu\mathrm{s}$, it is $T_V = 963 \pm 15\,\mathrm{ns}$. For currents, widths have great uncertainity where the peak is low, but it is possible to evaluate a mean value for $\Delta t \geq 6\,\mu\mathrm{s}$, and it is $T_I = 968 \pm 28\,\mathrm{ns}$. Values from the two measurements are compatible and they are a good estimation of pulse time duration.

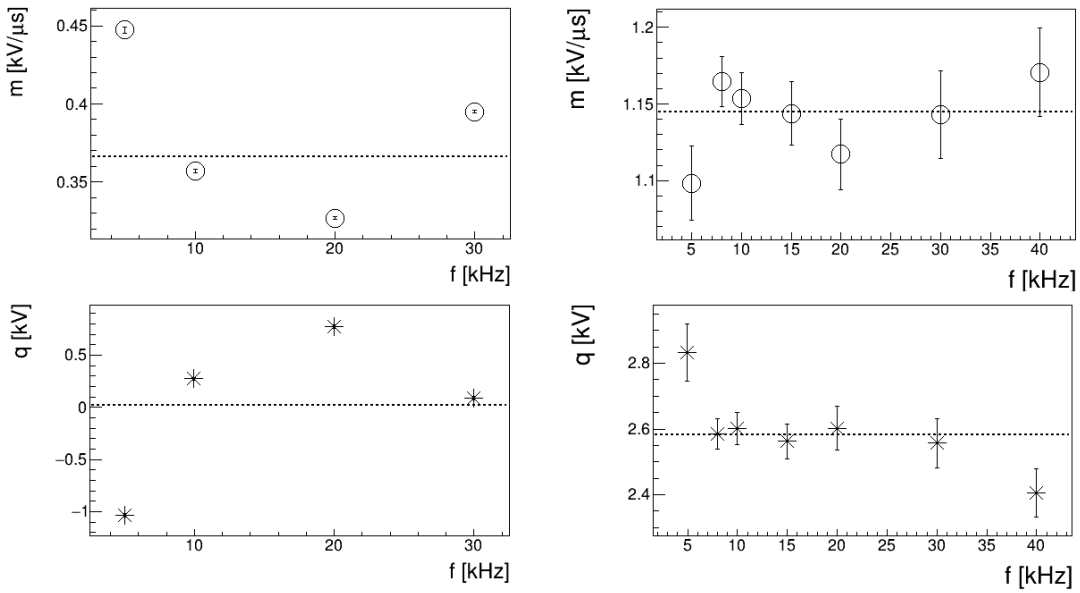

(a) Source A **(b)** Source B

Figure 1.10: We fit again voltage peak in function of Δt with a linear function $V_{peak} = m\Delta t + q$, in figure (a) and (b) there are fit parameters at different repetition rates for both sources. Dashed line is the average value of the parameter. Also when there is plasma we don't find specific behavior in parameters, so we conclude that output voltage doesn't depend on pulse repetition rate.

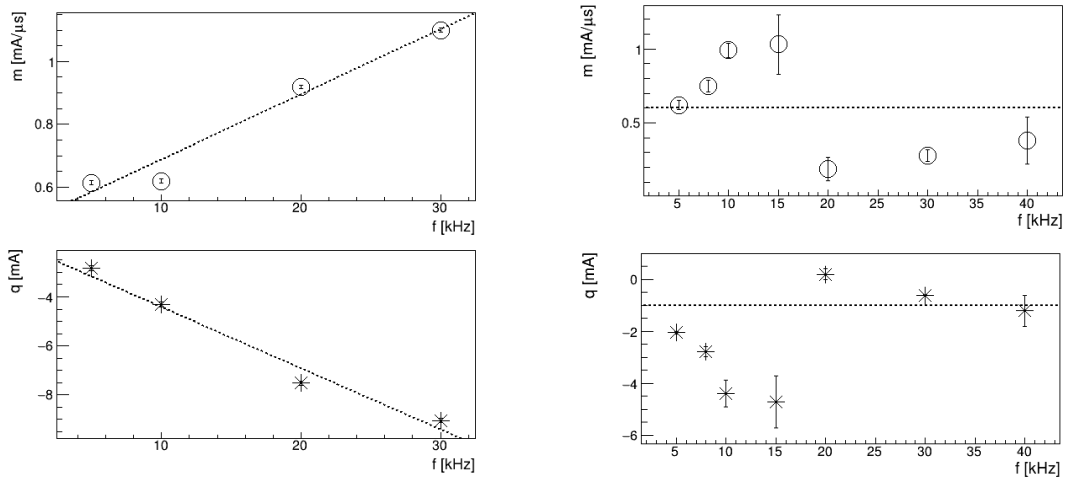

(a) Source A **(b)** Source B

Figure 1.11: We fit also current peaks with a linear function $I_{peak} = m\Delta t + q$, in figure we see fit parameters at different pulse repetition rates for both sources. For prototype **A** we find a linear dependency from f, in dashes in the figure. For prototype **A** we find again a random displecment around the average value.

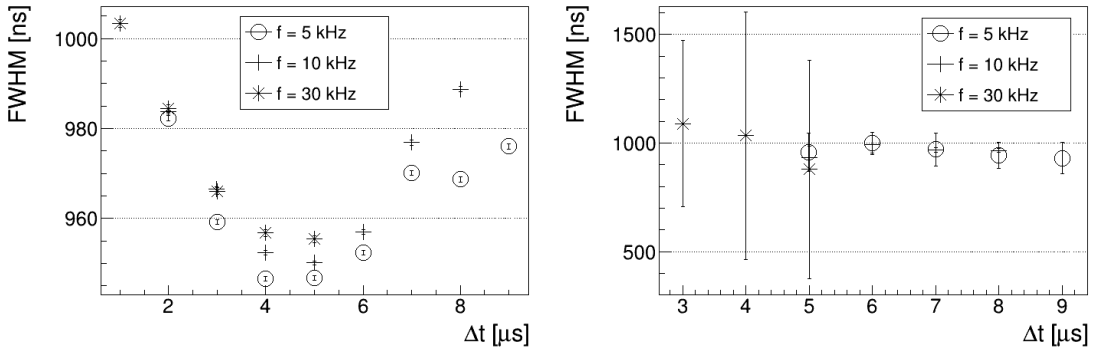

(a) Voltage **(b)** Current

Figure 1.12: FWHM of voltage and current pulses varying opening time, for different pulse repetition rates.

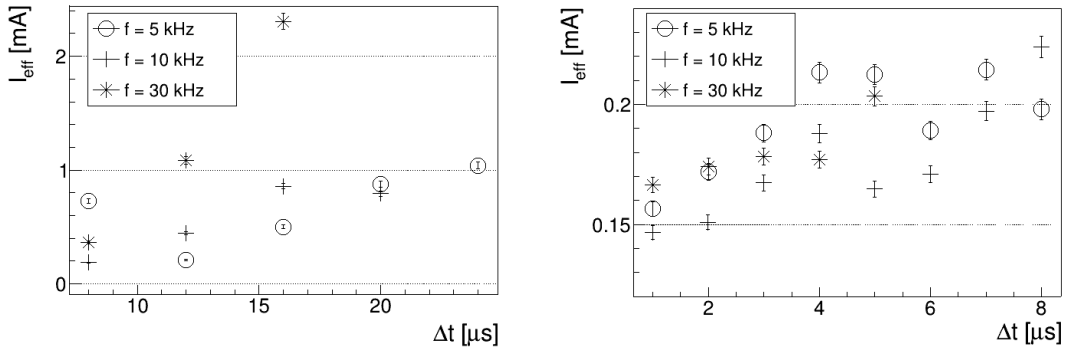

(a) Source A **(b)** Source B

Figure 1.13: Effective current values measured for a time interval of 1 ms.

1.3.3 Effective current

Current effects in applications on biological tissues have to take into consideration current intensity in a time interval tipically larger then the pulse widths used in our sources ([13], [2]). It's possible to estimate an effective current that is more appropriate to take into consideration when evaluating damage due to currents, as a mean of current intensity in a defined time interval calculated with equation 1.1, taking $t_2 - t_1 = 1\,\text{ms}$. The effective current takes into consideration that current values are very small for all the time between two pulses.

$$I_{\text{eff}} = \sqrt{\frac{1}{(t_2 - t_1)} \int_{t_1}^{t_2} I^2\, dt} \tag{1.1}$$

Figure 1.13 shows effective currents measured for both sources. Values are significantly smaller then maximum peak values, expecially for prototype **B** where oscillations after the main peak are smaller. The maximum value for the two prototypes is given by $I_{\text{eff}A} = 2.47 \pm 0.07\,\text{mA}$ and $I_{\text{eff}B} = 0.23 \pm 0.01\,\text{mA}$.

1.3.4 Plasma impedance

From voltage and current measuraments we can define plasma's electric behavior, in this subsection we try to estimate plasma impedance with measurements from prototype **B**. Voltage output from head's transformer can be modelized as a damped sine wave around the peak, as in equation 1.2, where V_{pulse} is the amplitude of the undamped pulse, τ is the characteristic damping time and f_{V_s} is the explicit parametrization of the frequency of the single pulse that we observe on measurements.

$$V_S = V_0 + V_{\text{pulse}} \sin(2\pi f_{V_s} t) e^{-t/\tau} \tag{1.2}$$

We can study how plasma impedance changes for different frequency pulse f_{V_s} to understand its electric behavior. Frequency pulse it's different for every opening time

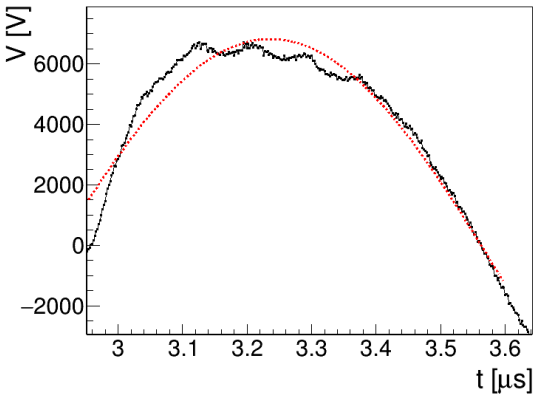

Figure 1.14: Example of a fit of voltage measurements with function 1.2.

of the circuit, Δt, but it's constant when changing pulse repetition rate, as explained before analyzing voltage outputs. In figure 1.14 there is an example of a peak fitted with the function in formula 1.2 while in figure 1.15 we show the resulting fit parameters for different Δt.

With higher opening times V_{pulse} is higher as expected, while f_{V_s} and τ have their own behaviors that depends from V_s. To estimate plasma's impedance it's useful to observe that voltage peak is quite large in time: it varies of less then 3% of peak's value in an interval of 150 ns around it. As voltage and current peaks times differs always by a time interval $|t_{V_p} - t_{I_p}| \leq 150\,\text{ns}$, it's possible to assume $V_{t_{I_p}} \simeq V(t_{V_p})$, i.e. that voltage during the current peak maximum is equal to voltage peak value. With this approximation, we can study voltage peak values in function of current peak value, as in figure 1.16. We can have an estimation of average plasma resistance from a linear fit or for a particular Δt it's possible to estimate it as $R = \frac{V_p}{I_p}$. Results are shown in figure 1.17, changing opening times and changing frequency of single pulse f_{V_s}.

From the graphs it's possible to extrapolate that plasma resistance goes from $2.98 \pm 0.11\,\text{M}\Omega$ to $11.82 \pm 2.19\,\text{M}\Omega$, with near constant values in the range of opening times $7-9\,\mu\text{s}$. From a deeper analysis and specific measures it could be possible to expand the analysis here presented and estimate plasma's electrical capacitance or induttance.

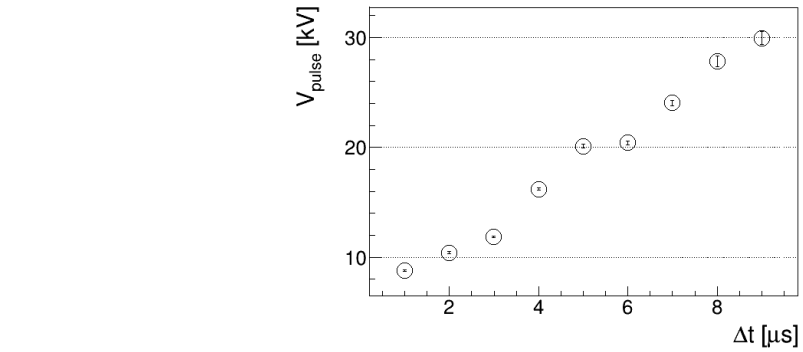

(a) V_{pulse}

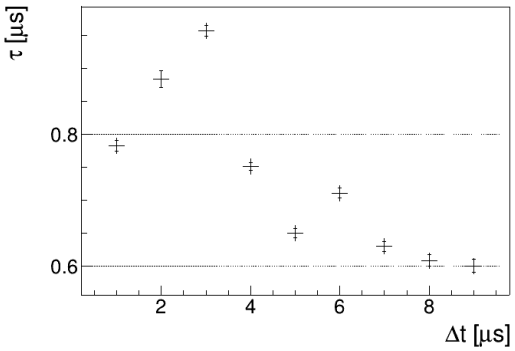

(b) τ

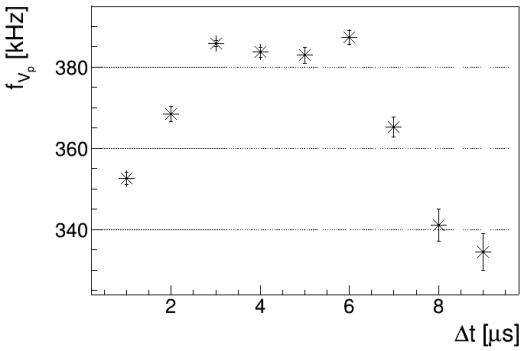

(c) f_{V_s}

Figure 1.15: Dumped sin fit parameters, as in equation 1.2, for pulses with $f = 8\,\text{kHz}$ and different Δt.

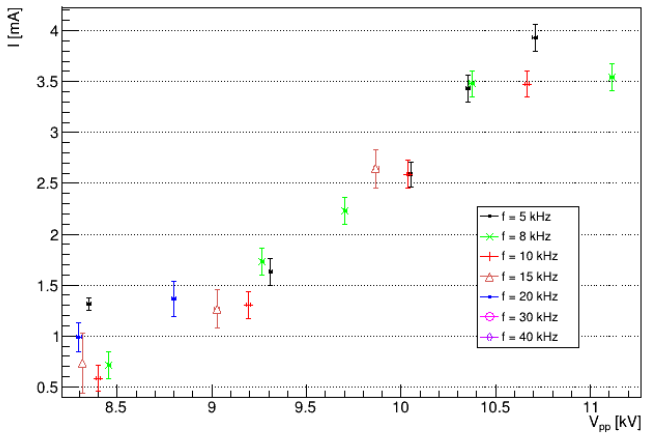

Figure 1.16: Voltage peak values against current peak values for different Δt and f.

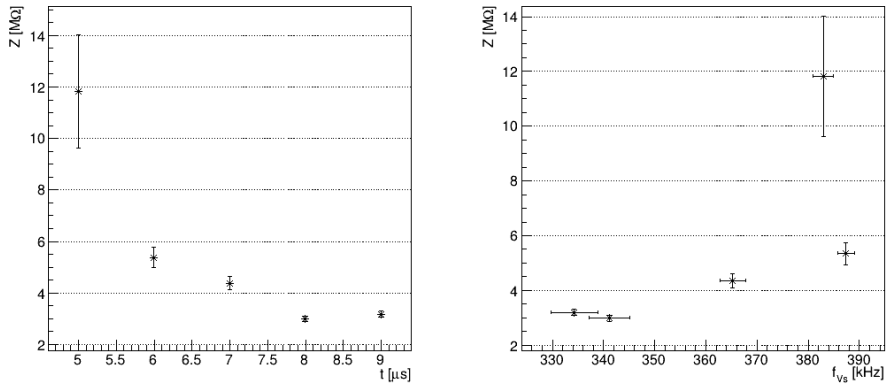

Figure 1.17: Impedance module estimation for different opening times (left) corresponding to different frequencies fit parameter (right).

Bibliography

[1] Gianluca De Masi et al. "Plasma Coagulation Controller: A Low- Power Atmospheric Plasma Source for Accelerated Blood Coagulation". In: *Plasma Medicine* 8.3 (2018), pp. 245–254. ISSN: 1947-5764.

[2] Cecilia Piferi. "Caratterizzazione di sorgenti di plasma per applicazioni biomediche". 2016/17.

[3] *Coils core datasheet*. URL: https://www.mouser.it/datasheet/2/400/e_32_16_9-1527777.pdf.

[4] J. Upadhyay et al. "Development of high-voltage pulse generator with variable amplitude and duration". In: *Review of Scientific Instruments* 85.6 (2014), p. 064704. DOI: 10.1063/1.4884883.

[5] Julien Jarrige, Mounir Laroussi, and Erdinc Karakas. "Formation and dynamics of plasma bullets in a non-thermal plasma jet: influence of the high-voltage parameters on the plume characteristics". In: *Plasma Sources Science and Technology* 19.6 (2010), p. 065005. DOI: 10.1088/0963-0252/19/6/065005. URL: https://doi.org/10.1088%2F0963-0252%2F19%2F6%2F065005.

[6] T Darny et al. "Analysis of conductive target influence in plasma jet experiments through helium metastable and electric field measurements". In: *Plasma Sources Science and Technology* 26.4 (2017), p. 045008. DOI: 10.1088/1361-6595/aa5b15. URL: https://doi.org/10.1088%2F1361-6595%2Faa5b15.

[7] *ROOT documentation for TVirtualFFT class*. URL: https://root.cern.ch/doc/master/classTVirtualFFT.html.

[8] R. Brun. *ROOT documentation for Landau() function*. 1995. URL: https://root.cern.ch/doc/master/namespaceTMath.html#a656690875991a17d35e8a514f37f35d9.

[9] U. Kogelschatz, B. Eliasson, and W. Egli. "Dielectric-Barrier Discharges. Principle and Applications". In: *Journal de Physique IV Colloque* 07.C4 (1997), pp. C4–47–C4–66. DOI: 10.1051/jp4:1997405. URL: https://hal.archives-ouvertes.fr/jpa-00255561.

[10] Takaaki Tomai, Tsuyohito Ito, and Kazuo Terashima. "Generation of dielectric barrier discharge in high-pressure N2 and CO2 environments up to supercritical conditions". In: *Thin Solid Films* 506-507 (2006), pp. 409 –413. ISSN: 0040-6090. DOI: https://doi.org/10.1016/j.tsf.2005.08.101.

[11] Lewi Tonks and Irving Langmuir. "A General Theory of the Plasma of an Arc". In: *Phys. Rev.* 34 (6 1929), pp. 876–922. DOI: 10.1103/PhysRev.34.876. URL: https://link.aps.org/doi/10.1103/PhysRev.34.876.

[12] M.A. Lieberman and A.J. Lichtenberg. *Principles of Plasma Discharges and Materials Processing*. Wiley, 1994. ISBN: 9780471005773. URL: https://books.google.it/books?id=-cloQgAACAAJ.

[13] Stephanie Tümmel et al. "Low Temperature Plasma Treatment of Living Human Cells". In: *Plasma Processes and Polymers* 4.S1 (2007), S465–S469. DOI: 10.1002/ppap.200731208. eprint: https://onlinelibrary.wiley.com/doi/pdf/10.1002/ppap.200731208. URL: https://onlinelibrary.wiley.com/doi/abs/10.1002/ppap.200731208.